Three-Dimensional Numerical Investigations on Lift and Drag Characteristics of Bird Wing Performing Flapping Motion

Amit Soni*, Harikrishnan S, Shaligram Tiwari
Department of Mechanical Engineering
Indian Institute of Technology Madras
Chennai-60036, India
Email: *amitthermaliitm@gmail.com

ABSTRACT

Present work carries out numerical investigations for 3-D model of flapping bird wing (owl) by use of commercial software ANSYS Fluent 15.0. In past, mostly standard air foil has been used to study flow characteristics of flapping motion. In the present study, geometry selection of owl wing has been done based on similar research reported in literature. Computations are carried out to simulate lift and drag characteristics of owl wing for different parameters, such as Reynolds number, angle of attack, frequency and amplitude. In the computational domain, dynamic meshing has been used to impart motion to the wing with the help of User Defined Function. Spring based smoothing function is selected for smoothing during dynamic motion of the wing. Literature reports that propulsive power can be generated by the flapping motion of wing beyond certain value of flapping frequency. Flapping motion in 3-D can be considered as a combination of both rotational and translational motions. For simplicity, the rotational motions are assumed to be present only about two axes, namely about stream-wise and span-wise directions. Effect of phase difference between the two rotational motions has been investigated and presented in the form of force coefficient ratio (R), which is the ratio of mean lift coefficient to mean drag coefficient. Critical value of Reynolds number has been computed at which the value of ratio R becomes equal to unity. Results show that an increase in flapping frequency is associated with a decrease in the value of mean drag coefficient.

INTRODUCTION

Nature has its best aerodynamic design, in the form of bird which is a result of continuous adaptation and evolution. Flying is complex phenomenon and requires that all of these phenomena should work in unison. During flying Reynolds number normally falls in the range of $10^3<10^6$ [1]. Understanding of natural flight, thus depends upon the behavior of wings at low Re, where laminar separation occurs and flow characteristics are strong function of Re at both steady and unsteady flight conditions. Bird wing performs weaker as compared to conventional air foil and also has lower efficiency[2]. Species share a common methodology for flying and swimming, i.e. a coupled motion to generate thrust. Thrust generation is based on amplitude, flapping frequency, Reynolds number and amplitude. Literature shows that species during flapping or swimming do not control parameters such as amplitude and frequency actively, instead they select to swim/ fly close to range of St = 0.20 to 0.4 [3]. Phase portrait for 2-D case has been studied and existence of limit cycle has been confirmed [4] for different initial conditions. If flying and swimming in nature represent a process with limit cycle, subtle but fundamental shift is needed to understand natural flying. Two-way coupled problem (fluid and wing) of natural flying could not be truly modeled either by simulations or experiments. It may happen that during study mean velocity of fluid is not adjusted to that observed during oscillations of wing and flow characteristics become different from freely flying conditions. Actually, overall efficiency of natural flyer is a result of various flapping and non-flapping aerodynamic surfaces like body, tail and fuselage. Interaction of wing with vortices shed by the body plays an important role during flying [5]. To mimic natural flying, add-ons can be added to wing[6]. which reduce drag and offer stability to the system.

For present simulation, scaled geometry has been taken as reported [7]. For non-flapping motion, effects of Re have been observed and mean drag coefficient has been confirmed in the range of 0.02-0.13 [8]. For comparative study, different wing shapes of different birds have been simulated. Effect of phase lag between the span-wise and stream-wise directions has been studied. Flapping frequency can be considered as one of the major factors in flapping flight. Time-dependent signal of drag coefficient has been plotted for different values of flapping frequency.

NOMENCLATURE

A	Projected surface area of wing
C_d	Coefficient of drag
C_l	Coefficient of lift
Re	Reynolds number
St_c	Strouhal number
T	Time period of flapping

U_∞ Mean free stream velocity
c_{mean} Mean chord length
L Wing length
t Dimensional time
u Velocity component in x-direction flow direction
v Velocity component in y-direction
w Velocity component in z-direction

Greek

α Angle of attack
f Flapping frequency
ρ_{air} Density of air
τ Non-dimensional time

Abbreviations

SIMPLE	Semi implicit pressure linked equations
UDF	User defined function
RMS	Root mean square

PROBLEM STATEMENT

Computational domain used for numerical investigations has been shown in Fig. 1. Length of the domain along flow direction is taken as $L_1 = 20c_{\text{mean}}$, along span wise direction as $L_3 = 10c_{\text{mean}}$ while $L_2 = 10c_{\text{mean}}$. Figure.2 shows the geometry of owl wing used for present study. Inlet velocity is based on mean chord length, i.e. $\text{Re} = \frac{\rho U c_{\text{mean}}}{\mu}$. Here flapping motion is assumed as rotational motion about x-axis and z-axis. Equations of motion about these axes are

$$\theta_x = \theta_{x_0} \sin(2\pi ft) \quad (1)$$

$$\theta_z = \theta_{z_0} \sin(2\pi ft + \phi) \quad (2)$$

Flapping cycle can be obtained by keeping θ_y constant and then an imaginary closed curve can be drawn, which is merely a representation of flapping pattern as shown in Fig. 3. In Fig.3, amplitude about x- axis varies from - 5° to 5° and about z-axis vary from - 2° to 2°, here value of ϕ is taken as 90°. Figure 3 shows the flapping cycle pattern and thus presents flapping cycle analogy. Pivot point for simulation has been taken at $0.3c_{\text{mean}}$ from leading edge at mid-span. Simulations have been carried out for both with and without phase difference between rotational motion about x and z-axes. X-axis represents the flow direction and z-axis represents span-wise direction.

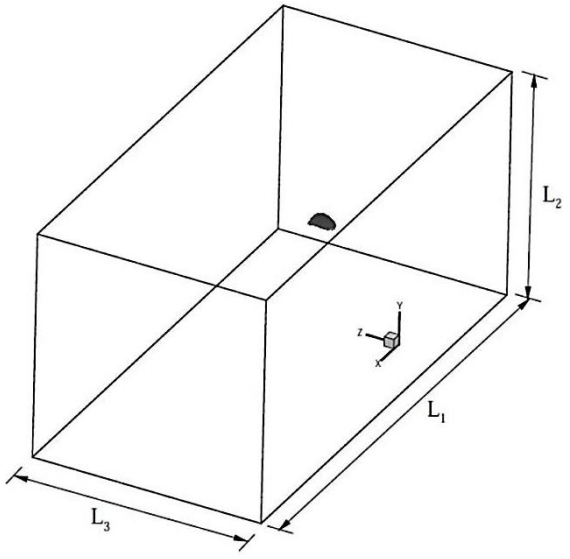

Fig. 1: Domain used for computations

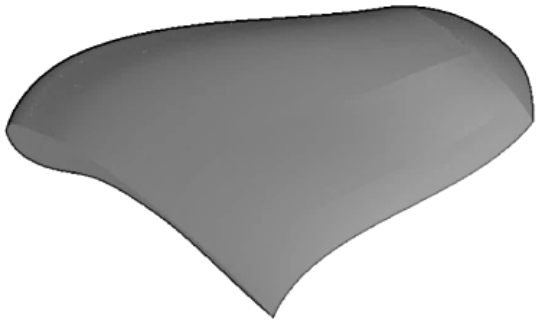

Fig. 2: Geometry of owl-wing used for simulation

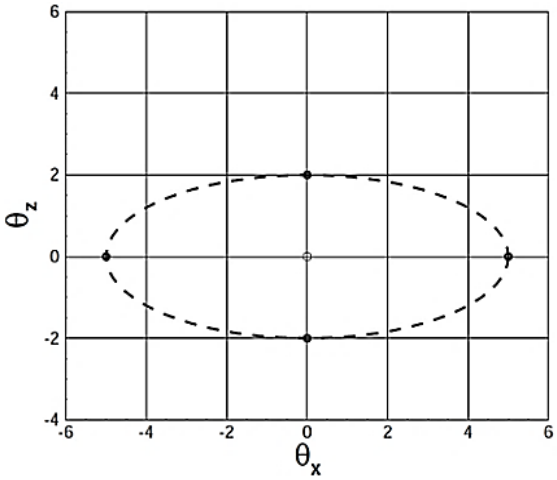

Fig. 3: Flapping cycle indicating variation of amplitude along x-axis from - 5° to 5° and about z-axis from - 2° to 2°

GOVERNING EQUATIONS AND BOUNDARY CONDTITONS

Governing equations

3-D governing equations used for numerical computations are incompressible continuity and momentum equations and are given as

$$\nabla.\vec{V} = 0 \tag{3}$$

$$\frac{\partial \vec{V}}{\partial t} + \vec{V}.\nabla\vec{V} = -\frac{1}{\rho}\nabla p + \nu\nabla^2\vec{V} \tag{4}$$

where velocity vector $\vec{V}$ is has components u, v and w in x, y and z-directions respectively while ρ and ν are density and kinematic viscosity of surrounding fluid medium.

Boundary conditions

1 Inlet: Uniform velocity condition, i.e. $u = U_\infty$; v = w = 0.

2 Outlet: Pressure outlet condition $p = p_\infty$

3 Side, top and bottom walls: Free-slip boundary conditions

4 Owl wing surface: No-slip boundary condition

GRID MESH AND NUMERICAL METHODOLOGY

For simulating the flow situation, the computational domain is divided into regions with two types of grids. The grids close to wing surface have tetrahedral structure which is used for the dynamic meshing. The structured and unstructured grids are separated by the interface. Schematic of the grid mesh has been shown in Fig. 4 where the tetrahedral grids are denser near the corner of wing to capture flow characteristics. Grid-independence has been confirmed (Fig. 5) by changing number of nodes over the mean chord length and for simulations wherefrom N_{cmean} = 100 have been chosen for all computations. User defined function (UDF) has been incorporated in ANSYS Fluent 15 to impart dynamic motion to the wing.

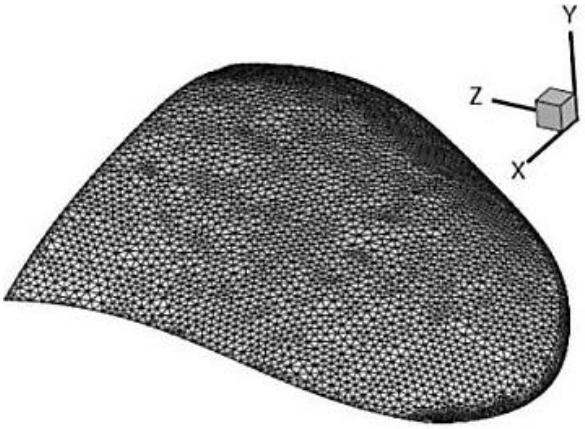

Fig. 4: Schematic of grid mesh for owl-wing

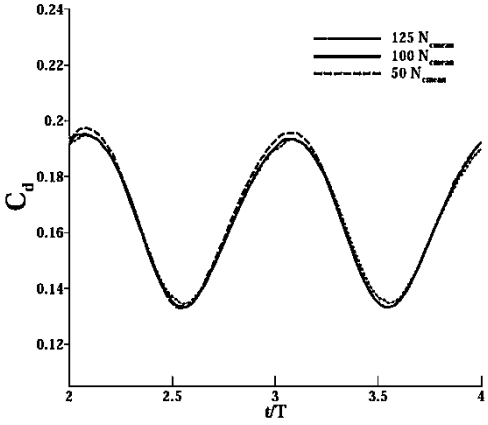

Fig. 5: Variation of drag coefficient for different number of grids along mean chord

RESULTS AND DISCUSSION

Validation of computations

Numerical results from present computations have been compared with those reported from experimental and numerical results of [9]. Mean value of force coefficients are taken after t = 13s to validate with the experimental results. For present computations, rectangular plate with same geometrical specification has been taken and variations of mean force coefficient are plotted against different values of angle of attack. Fig. 6(a) shows the comparison of C_d with respect to angle of attack of rectangular plate with aspect ratio 2 at Re = 100. For flapping case, numerical results from present computations have been compared for flapping airfoil with those reported from experimental study of [10]. Figure 6(b) shows comparison of non-dimensional velocity in y-direction measured at a distance of x/c= 1 for non-dimensional frequency of 6.6, also known as 'reduced frequency. Simulations have been done over 2-d owl wing at Re = 23000 and comparison of lift coefficients for different values of angle of attack have been done as shown in Fig.6 (c) against [11].

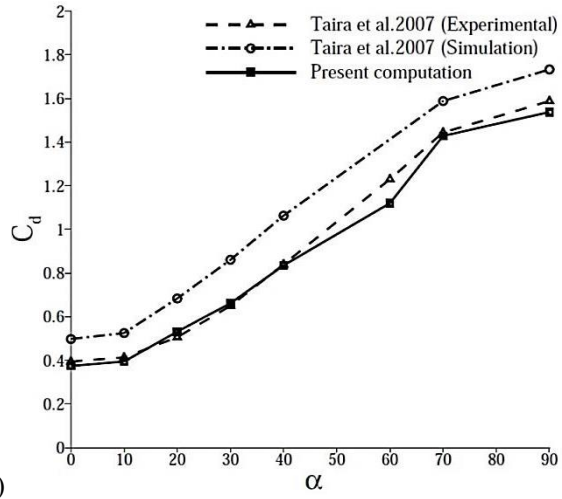

(a)

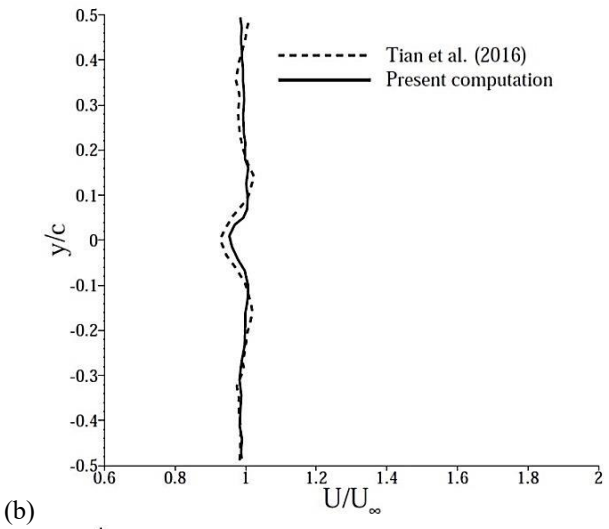

(b)

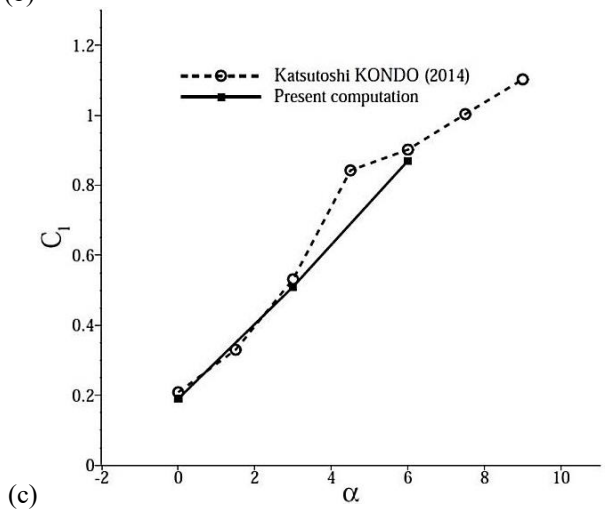

(c)

Fig.6: Comparison of (a) drag coefficient for different values of angle of attack at Re = 100 [9] (b) non-dimensional velocity profile at different non-dimensional locations of y-direction as reported in [10] and (c) lift force coefficient for different values of angle of attack at Re = 23000 for 2-D owl wing as reported in [11]

TRENDS AND RESULTS

Comparative study of different wing models

For the same flapping motion, flow dependent characteristics have been investigated for different types of wings, i.e. both standard and biological wings. It has been seen that biological wing produces less drag as compared to standard rectangular wing. The geometrical enhancement may reduce drag force experienced by the body which is dependent on profile of the wing. Figure 7 shows that for rectangular wing drag has higher values as compared to other two wings.

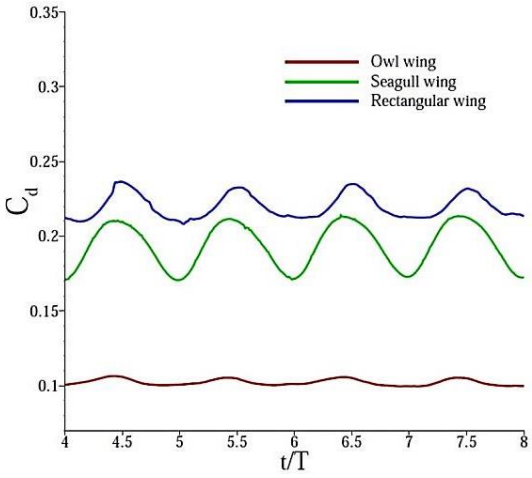

Fig. 7: Instantaneous drag signal for different wing models at Re = 5000

Lift signal for different values of Re at frequency of 1 Hz

Time dependent signals at different values of Re are shown in Fig. 8 (a). It has seen that with increase in Re magnitude of coefficient of lift signal decreases because at low Re there is a saddle point formation at the trailing edge of owl wing, which is not observed for higher values of Re. When phase difference between the two rotational motions is kept at 90^o, in which rotation about z-axis leads, mean lift coefficient increases which is shown using solid line with red dot for Re = 5000. Investigations have been done for Re ranging from 1000 to 5000. Flow characteristics of owl wing have been shown in Fig. 8(b), upper figure shows the case without phase difference and lower one for with phase difference. The circulation present below the wing surface for owl wing with no phase difference leads to reduction in value of lift. With difference in phase of 90^o it has seen that value of *R* becomes 1.57 at Re = 5000 whereas *R* becomes 1 at same Re for flapping motion without phase difference Fig. 8 (c). Critical Re for present computation has been occurred at Re = 5000, for a case without phase difference between flapping motion about x and z-axis.

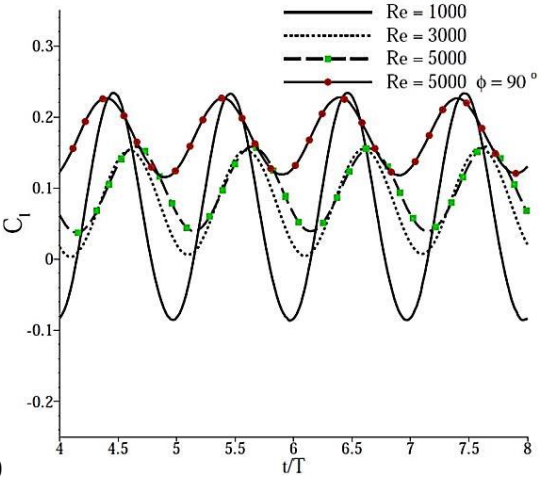

(a)

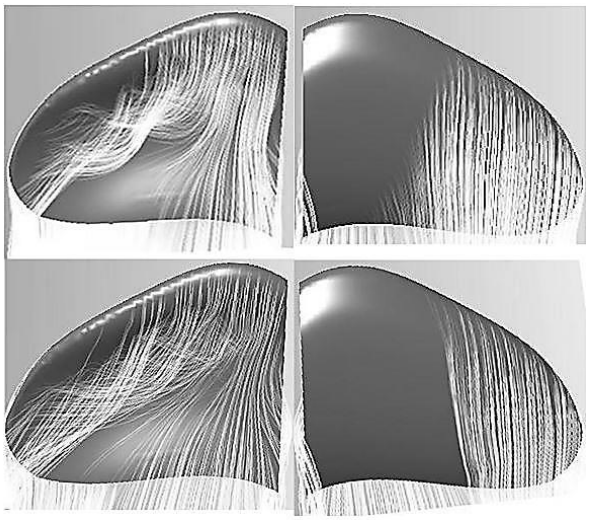

(b)

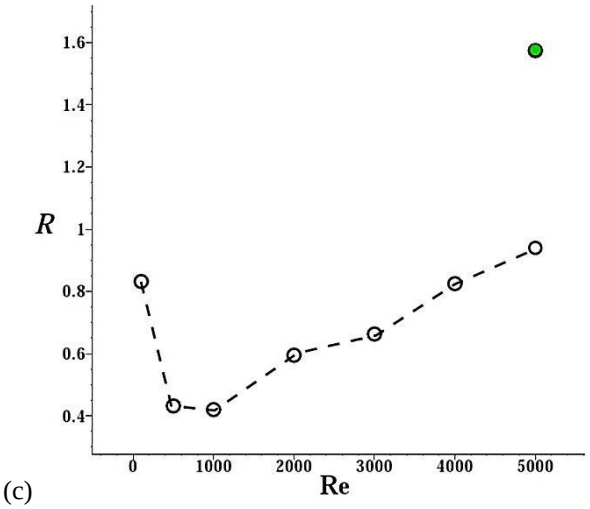

(c)

Fig. 8: Variation of (a) time dependent lift signal for different values of Re and phase difference (b) upper figure shows circulation zone without phase difference and lower figure shows circulation zone with phase difference at Re = 5000 and (c) variation of force coefficient ratio R against Re where green dot indicates flapping motion with phase difference of 90^o

Effect of flapping frequency

Here computations are performed for different frequencies at Re = 2000 for owl wing. The wing has been imparted rotational motion only about x-axis. Figure 9 shows instantaneous drag signal for the owl wing. It is observed that with the increase in flapping frequency the mean drag coefficient reduces for a given Re. At f = 4 Hz, mean drag coefficient ratio is 0.14 and at f = 12 Hz, it is 0.055 as presented in Fig. 10. Drag reduction by increasing frequency shows an interesting behavior where conversion from momentum deficit wake to momentum sufficit wake is observed to take place.

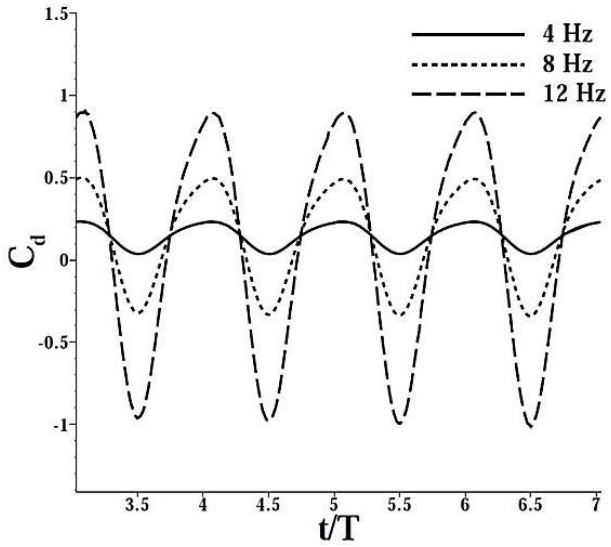

Fig. 9: Instantaneous drag signal for different values of flapping frequency at Re = 2000

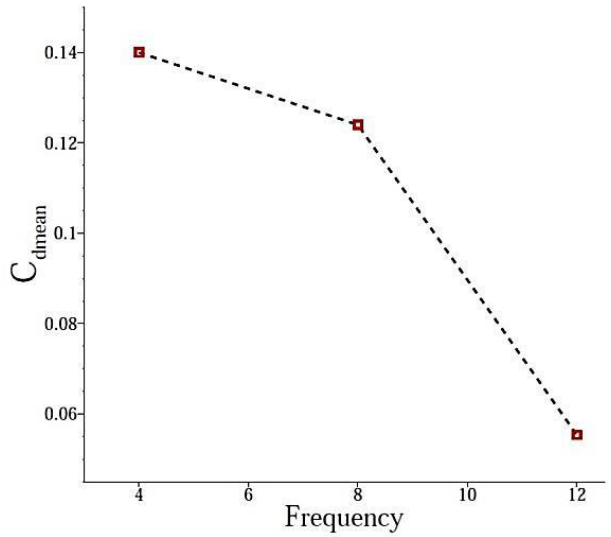

Fig. 10: Variation of mean drag coefficient for different values of flapping frequency at Re = 2000

CONCLUSION

Numerical investigations have been carried out for different types of wing models. Biological wing produces less drag as compared to standard wing shape. A phase difference of 90^o enhances the lift coefficient for given wing motion. Flapping frequency plays a vital role in flapping flights where with increase in flapping frequency drag force on wing reduces. Natural flyers show the best possible aerodynamic design which is really difficult to mimic. Present computations predict the fundamental behavior of flapping wing. Effect of flexibility of wing and study of different wing parts can form the extended part of investigations for further enhancement in aerodynamic performance of the commercial aircraft.

REFERENCES

[1] K. D. von Ellenrieder, K. Parker, and J. Soria, "Fluid mechanics of flapping wings," *Exp. Therm. Fluid Sci.*, vol. 32, no. 8, pp. 1578–1589, 2008.

[2] M. A. Aldheeb, W. Asrar, E. Sulaeman, and A. A. Omar, "A Review on Aerodynamics of Non- flapping Bird Wings," *J. Aerosp. Technol. Manag.*, vol. 8, pp. 7–17, 2016.

[3] G. K. Taylor, R. L. Nudds, and A. L. R. Thomas, "Flying and swimming animals cruise at a Strouhal number tuned for high power efficiency," *Nature*, vol. 425, pp. 707–711, 2003.

[4] R . A . Skop and S . Balasubramanian, "A new twist on an old model for vortex-excited vibrations," *J. Fluids Struct.*, vol. 11, pp. 395–412, 1997.

[5] M. S. Triantafyllou, G. S. Triantafyllou, and D. K. P. Yue, "Hydrodynamics of fishlike swimming," *Annu. Rev. Fluid Mech. 2000.*, vol. 32, pp. 33–53, 2000.

[6] N. M. Bakhitan, H. Bbinsky, A. L. R. Thomas and G. k. Taylor, "The Low Reynolds number aerodynamics of leading flaps,", *in 45th AIAA Aerospace Sciences Meeting and Exhibit8 - 11 January 2007, Reno, Nevada*

[7] T. Liu, K. Kuykendoll, R. Rhew, and S. Jones, "Avian Wing Geometry and Kinematics," *AIAA J.*, vol. 44, no. 5, pp. 954–963, 2006.

[8] P. C. Withers, "An aerodynamic analsis of bird wing as a fixed aerofoils," *J. Exp. Biol.*, vol. 96, pp. 7167–7174, 1991.

[9] K. Taira, W. B. Dickson, T. Colonius, and M. H. Dickinson, "Unsteadiness in Flow over a Flat Plate at Angle-of-Attack at Low Reynolds Numbers," *AIAA J.*, pp. 710–726, 2007.

[10] W. Tian, A. Bodling, H. Liu, J. C. Wu, G. He, and H. Hu, "An experimental study of the effects of pitch-pivot-point location on the propulsion performance of a pitching airfoil," *J. Fluids Struct.*, vol. 60, pp. 130–142, 2016.

[11] K. Kondo, "Computational comparative study for design of low Reynolds number airfoil," in *29 th Congress of the International Council of the Aeronautical Sciences*, 2014, pp. 1–10.